

Decoding Quantum LDPC Codes using Collaborative Check Node Removal

Mainak Bhattacharyya and Ankur Raina

Department of Electrical Engineering and Computer Science
Indian Institute of Science Education and Research Bhopal, India
Email: {mainak23, ankur}@iiserb.ac.in

Abstract—The fault tolerance of quantum devices requires on-par contributions from error-correcting codes and suitable decoders. One of the most explored error-correcting codes is the family of Quantum Low-Density Parity Check (QLDPC) codes. Although faster than many of the reported decoders for QLDPC codes, iterative decoders fail due to the colossal degeneracy and short cycles intrinsic to these codes. We present a strategy to improve the performance of the iterative decoders based on a collaborative way to use the message passing of the iterative decoders and check node removal from the code’s Tanner graph. We use the concept of bit separation and generalize it to qubit separation. This gives us a metric to analyze and improve the decoder’s performance towards harmful configurations of QLDPC codes. We present a simple decoding architecture to overcome iterative decoding failures by increasing the separation of trapped qubits without incurring any significant overhead.

I. INTRODUCTION

Quantum Low-Density Parity Check (QLDPC) codes stand as the most suitable candidate for achieving practical fault tolerance with their low overhead [1] and good error correction properties [2], [3]. A good error-correcting code refers to code that has a constant rate and shows linear or constant distance scaling. In comparison with the classical LDPC codes, QLDPC code constructions are less trivial. The first set of construction towards achieving the same was the hypergraph product (HGP) codes by Tillich and Zémor [3]. These QLDPC codes achieve a constant rate and a quadratic distance scaling (that is, $d \propto \sqrt{n}$) as an outcome of the tensor product between any two classical codes. The well known Toric code is a class of HGP code itself. More recent studies have presented the first constructions of asymptotically good QLDPC codes [4], [5]. For instance, Panteleev and Kalachev first proposed a generalization of the HGP construction [6], which later they renamed to Lifted Product codes [2], reporting the first QLDPC codes with almost linear distance.

The performance of these QLDPC codes are far from optimal under the current decoders available. Unlike the classical LDPC codes, high degeneracy and short cycles present in the Tanner graph of the code poses a big hurdle during the decoding. Particularly iterative Belief Propagation (BP) based decoders completely fail while decoding these highly degenerate quantum codes. The state-of-the-art QLDPC decoder with a mammoth amount of success rate is the BP-OSD decoder [6]. It uses a post processing classical

method based on the Ordered Statistics Decoding (OSD), to solve an inverse based problem to exhaustively find minimum weight error patterns that satisfy the syndrome. Although very accurate, it has a $\mathcal{O}(n^3)$ time complexity in the number of physical qubits n used by the error correcting code. Although, more accurate and higher order decoding of the same is too expensive for using in any practical cases. Recent attempts are made to achieve a similar accuracy with reduced time complexity [7], [8]. Also there have been certain decoders which in part, use BP and leverages from the properties of large codes, such as expansion to post-process the trapped BP outputs [9].

Different harmful configurations intrinsic to the QLDPC codes are considered as the main source of iterative decoding failures. Previous attempts were made based on the knowledge of these configurations and helping the decoder learn or facilitate asymmetric message passing rules to avoid failures [10]–[12]. In this work, we present a simple approach to assist the iterative decoder without the knowledge of these configurations. In this way we save a lot of effort towards exhaustive analysis and expensive learning based resource exploitation. We provide a notion of the *qubit separation* and show that removing certain mis-satisfied and symmetric check nodes (i.e. stabilizers) can improve the iterative decoder’s performance. We show that the decoder’s performance is directly linked with increased separation of the qubits belonging to the harmful configuration sets. We also leverage from the intrinsic degeneracies to estimate the separation of qubits belonging to symmetric stabilizers sets. We show a probabilistic check node removal approach like [13] offers highly separated qubits and thus can ensure a better performing decoding architecture than that of the decoders involving only iterative message passing. We observe that the proposed collaborative architecture incurs very little overhead to the overall decoding process compared to the existing post-processing methods and offers a performance bridge between iterative and the iterative + post-processing-based decoders.

The paper is organized as follows: In Section II, we describe the classical and quantum error correction process and also provide necessary details of the Generalized Hypergraph Product (GHP) code that we use primarily for testing and

analyzing the decoder. In Section III, we analyze the harmful configurations that arise for GHP quantum code resulting in decoding failures and discuss how one can break pass those failures by increasing the separation of the trapped qubits. Finally, we discuss the proposed collaborative decoding in Section IV and show that the proposed sub-decoding mode can indeed improve from the trapped error floor region of a BP *min-sum* decoder and compare the performance of the proposed work with BP and BP-OSD0 using some memory experiments for the $[[882, 24]]$ and $[[1270, 28]]$ GHP codes.

II. PRELIMINARIES

We now briefly discuss the classical and quantum error correction process and summarize the *min-sum* BP decoder.

A. Classical Error Correction

Classical error correcting codes are a typical binary map, which encodes k bits of information into n bits of codeword c , where $n > k$. The error correction mechanism can be expressed through the generator matrix \mathbf{G} or the parity check matrix \mathbf{H} . The former method uses the fact that the rows of \mathbf{G} span the set of all codewords \mathcal{C} . The latter defines a code through the null space of \mathbf{H} , that is, any codeword $c \in \mathcal{C}$:

$$\mathbf{H}c^T = 0 \pmod{2}. \quad (1)$$

This establishes the foundation to identify and correct errors. For example, if there is an error η occurred, the codeword becomes erroneous, i.e., $c \rightarrow y := c + \eta$ and therefore Eq. (1) gets violated. Knowledge of the error η is often deciphered using the syndrome s computed using y and \mathbf{H} as

$$\mathbf{H}y^T = s. \quad (2)$$

There exist nonzero syndromes only for errors η with a Hamming weight upper bounded by $\text{wt}(\eta) < d$, where d is the minimum distance of the classical code. A decoder typically leverages the syndrome information and predicts the error occurred but the performance of the decoder is often restricted by both the decoding algorithm as well as the constraints imposed by the minimum distance of the code.

B. Quantum Error Correction

Quantum error correcting codes similar to classical codes use redundancy to encode the information of k logical qubits into n physical qubits. The fundamental errors that qubits suffer include continuous errors, unlike the bit flips in the classical case. A typical error in a quantum system can be expressed as a linear combination of errors in the Pauli set $\{I, X, Y, Z\}$. The Pauli- X operator acts similarly to the classical bit flip error by flipping the bit-state of a qubit. Meanwhile, the Pauli- Z operator changes the phase of a quantum state. The encoded logical qubit state $|\psi\rangle_L$ belongs to the space of $(+1)$ eigenstates of a set of Pauli operators $\mathcal{S} \subset \mathcal{G}_n$, called the stabilizers of the code. Any error must anti-commute with one of the stabilizers for the decoder to be able to detect it. A one-to-one map exists between the stabilizer set and parity checks matrices for a quantum code where the rows

map to the stabilizers of the code. For instance, if a quantum $[[n, k, d]]$ code has a stabilizer set $\mathcal{S} = \{s_1, s_2, \dots, s_{n-k}\}$. The parity check matrix can be defined by stacking the stabilizers in the rows to form the matrix

$$\begin{bmatrix} s_1 \\ s_2 \\ \vdots \\ s_{n-k} \end{bmatrix}.$$

The symplectic format allows a binary representation of the parity check matrix of the above representation. In this format, each of the n qubit Pauli operators is represented using a $2n$ bit string. For example, one qubit Pauli operator follows

$$X \mapsto (1|0), \quad (3)$$

$$Y \mapsto (1|1), \quad (4)$$

$$Z \mapsto (0|1). \quad (5)$$

The parity check matrix can be described in binary form as:

$$\mathbf{H} = [\mathbf{H}_X | \mathbf{H}_Z]. \quad (6)$$

For any valid code, the stabilizers must all commute with each other, requiring the following to hold:

$$\mathbf{H}_X \mathbf{H}_Z^T + \mathbf{H}_Z \mathbf{H}_X^T = 0. \quad (7)$$

This constrains the development of quantum codes. Particularly in this work, we focus on a very well-studied class of quantum codes called quantum low-density parity check (QLDPC) codes [14]. More specifically, we focus on the class of Calderbank-Shor-Steane (CSS) codes [15], [16] with a special property that the number of 1's in each row and column is upper bounded by a constant with the number of qubits going to infinity. This results in a very sparse parity check matrix, which is very efficient with respect to iterative decoding. The stabilizers of these codes are of the independent type, meaning they contain either Pauli- X or Pauli- Z operators and as a result, Eq. (6) takes a special form

$$\mathbf{H} = \begin{bmatrix} \mathbf{H}_X & \mathbf{0} \\ \mathbf{0} & \mathbf{H}_Z \end{bmatrix}. \quad (8)$$

This ensures that decoding can be performed independently for syndromes due to bit flips and the syndromes due to phase flips. Also, Eq. (7) can now be reduced to

$$\mathbf{H}_X \mathbf{H}_Z^T = 0. \quad (9)$$

Following this, we explore a special generalization of the HGP codes, with improved code properties that require specialized analysis.

C. Generalized Hypergraph Product (GHP) Codes

An intuitive way to construct QLDPC codes based on Eq. (9), is using two commuting matrices and stack them together to form the parity check matrix of the QLDPC code [17]. Panteleev and Kalachev use this intuition to propose a generalization of the standard hypergraphproduct codes [6]. In their work they consider two square matrices, elements of

which belongs to a ring called ring of circulants defined below in II.1.

Definition II.1 (Ring of Circulants). *A ring of circulant \mathbb{A}_L satisfies all the properties of a ring with its members being the circulant permutation matrices or sometimes referred to as the polynomials. The whole ring is characterized by a parameter called "lift", which is essentially the dimension of the permutation matrices.*

If the ring of circulants contains only null and identity, then the GHP CSS code reduces to HGP code. The parity check matrix of a GHP code is of the following form:

$$\mathbf{H}_X = [A, bI_m] \text{ and } \mathbf{H}_Z = [b^T I_n, A^T], \quad (10)$$

where A is a matrix $A = [a_{ij}]_{m \times n}$, such that $a_{ij} \in \mathbb{A}_L$ and $m = n$. Further, b is a polynomial in \mathbb{A}_L and I_m and I_n are diagonal matrices with its diagonal entries being the identity of the ring. For example, we will extensively use the $[[882, 24]]$ code discussed in [6], which uses

$$A = \begin{pmatrix} x^{27} & 0 & 0 & 0 & 0 & 1 & x^{54} \\ x^{54} & x^{27} & 0 & 0 & 0 & 0 & 1 \\ 1 & x^{54} & x^{27} & 0 & 0 & 0 & 0 \\ 0 & 1 & x^{54} & x^{27} & 0 & 0 & 0 \\ 0 & 0 & 1 & x^{54} & x^{27} & 0 & 0 \\ 0 & 0 & 0 & 1 & x^{54} & x^{27} & 0 \\ 0 & 0 & 0 & 0 & 1 & x^{54} & x^{27} \end{pmatrix}, \quad (11)$$

$$b = (1 + x + x^6) I_7, \quad (12)$$

where $x^i, \forall i \in \{1, \dots, L-1\}$ are the polynomials with its columns shifted by i from the identity. Also the lift for the ring is set as $L = 63$, thus all this polynomials are (63×63) matrices over \mathbb{F}_2 .

D. Iterative Decoding

We discussed in the previous sections that errors anti-commuting with the stabilizers result in non-zero syndrome and indicate the occurrence of errors. Based on the received syndrome s , the decoding problem is a search for the error, which maximizes the posterior probability:

$$\hat{e} = \arg \max_{e \in \mathcal{G}_n} P(e|s), \quad (13)$$

where, \hat{e} is the best estimate of the error e and \mathcal{G}_n is the set of all n -qubit Pauli operators. In case of quantum error correction, the optimal decoding is instead solving the following optimization:

$$\hat{e} = \text{any}(E) : E = \arg \max_{E \in \mathcal{E}} P(E|s), \quad (14)$$

where E is the coset of an error $e \in \mathcal{G}_n$ such that $E := e\mathcal{S}$. \mathcal{E} is a collection of all such possible cosets. The estimated error \hat{e} of Eq. (14) can be any operator from the maximum probability coset E , as members of a single coset has the same logical effect on the state.

Throughout this article we use iterative decoding and BP decoding in an equivalent manner. BP is an iterative

message-passing algorithm due to its continuous back-and-forth information-passing characteristics over a bipartite Tanner graph of the code. BP primarily evaluates the marginals of Eq. (13), i.e.

$$\hat{e}_i = \arg \max_{e_i \in \{e_1, e_2, \dots, e_n\}/e_i} P(e_i|s), \quad (15)$$

Therefore it so happens that the maximized \hat{e} in (13) does not always satisfy Eq. (14). Many variants of the BP algorithm exist, primarily depending on the application of the algorithm. We describe very briefly the *min-sum* algorithm, which we used for the numerical experiments and also offers better numerical stability than the others. This algorithm performs series of binary message passing from data qubit nodes to its adjacent check nodes and vice-versa, producing soft outputs for each data qubit nodes. We use u_i and v_j to denote the i^{th} data and j^{th} check nodes respectively. Also, we assume the notation $m_{a \rightarrow b}^k$ to portray message passed at the k^{th} iteration of the algorithm from node a to node b on the Tanner graph. Following we describe an overall brief summary of the standard message passing rule of the *min-sum* BP:

- 1) Initialization: Initially from each data qubits a message $m_{u_i \rightarrow v_j}^0$ is passed as follows:

$$m_{u_i \rightarrow v_j}^0 = \lambda_i = \log\left(\frac{1-p_i}{p_i}\right); \forall i, j : \mathbf{H}_{ji} = 1. \quad (16)$$

- 2) Check to data qubit messages: For the subsequent iterations, message $m_{v_j \rightarrow u_i}^k$ is passed from each check node to data qubits. Although note we exclude the message passing to the qubit node, which was immediately involved in message passing at $k-1^{\text{th}}$ iteration. We define a quantity $w = \min_{u_p: N(v_j)/u_i} \{|m_{u_p \rightarrow v_j}^{k-1}|\}$ and the message passed is as follows:

$$m_{v_j \rightarrow u_i}^k = (-1)^{s_j} \alpha \left(\prod_{u_p: N(v_j) \setminus u_i} \text{sign}(m_{u_p \rightarrow v_j}^{k-1}) \right) w, \quad (17)$$

where, α is a scaling factor and can affect the convergence and s_j is the syndrome value corresponding to the check node v_j .

- 3) Data qubit to check messages: Except the initialization as described, at each iteration k , the messages passed from data qubits to check nodes follows:

$$m_{u_i \rightarrow v_j}^k = \lambda_i + \sum_{v_p: N(u_i) \setminus v_j} m_{v_p \rightarrow u_i}^{k-1} \quad (18)$$

- 4) Hard decision: At the end of each iteration, a soft output is evaluated for each qubit node. The soft output represents the collective response received from all the check nodes and is as follows:

$$\gamma_i \leftarrow \lambda_i + \sum_{v_p: N(u_i)} m_{v_p \rightarrow u_i}^k. \quad (19)$$

If $\text{sign}(\gamma_i) = -1$, then the hard decision for data qubit i is $\hat{e}_i = 1$, otherwise $\hat{e}_i = 0$.

The whole process continues until all the unsatisfied checks are satisfied or a pre-determined number of message-passing iterations is reached, and the syndrome is still non-zero. In the former, the decoding is said to have succeeded, and the latter reflects a decoding failure. A cycle-free Tanner graph guarantees the success of BP within a finite number of iterations, although QEC offers plenty of short cycles along with inevitable degeneracies, which makes BP fail miserably. In the following section, we discuss one such case where some inherent configurations of the GHP code render BP an ineffective decoder.

III. TRAPPING SETS AND SEPARATION VECTORS OF GHP CODES

Iterative message passing-based decoders are vulnerable when it comes to certain error configurations. These are heavily studied and formally named as the Trapping sets (TS) and we will use \mathcal{T}_s to denote the set of data qubits that are trapped. If \mathcal{T}_s contains a data qubits and b odd degree stabilizer checks then it is a (a, b) trapping set of the code. We use the notation V_1 to describe the set of qubits $v \in \mathcal{T}_s$, such that v is adjacent to odd degree stabilizer checks. Note that there can be many possible configurations for any (a, b) TS, depending on the geometry of the code and the decoder under consideration.

A. Trapping set analysis

For QLDPC codes there exists two class of harmful TS configurations: Classical- type trapping sets (CTS) and Quantum trapping sets (QTS). The definitions of CTS and QTS are briefly covered in III.1 and III.2, which we adopt from [11].

Definition III.1 (Classical-type Trapping sets). *A classical-type trapping set is a set of qubits which either do not converge or they are adjacent to unsatisfied stabilizer checks after a predetermined number of iterations of a syndrome based iterative decoder.*

For example in Fig. 1(a), we show a $(3, 3)$ CTS obtained from the \mathbf{H}_Z of the same [[882, 24]] GHP code mentioned in (11). As can be seen from the qubit and check node indexing, the CTS is formed only due to the contributions of a particular circulant matrix, namely $b^T I_n$. This type of CTS formation is also discussed in [18]. The *min-sum* iterative decoder in II-D fails to converge in this scenario due to the symmetric message passing rules. For example, for a received syndrome $s = \{c_0, c_1, c_2, c_6, c_7, c_{12}\}$, the *min-sum* BP based decoder oscillates between an all-zero error pattern and an error pattern of $\{v_0, v_1, v_6\}$, as shown in Fig 2.

The other type of TS that often occurs in the QLDPC codes are the Quantum Trapping sets (QTS) as defined in III.2. These trapping sets do not have any odd-degree check nodes. Thus, a QTS with a number of data qubits is referred as a $(a, 0)$ trapping set. Fig. 1(b) shows a typical QTS formed for the same GHP code with 6 data qubits in \mathcal{T}_s .

Definition III.2 (Quantum Trapping sets). *A quantum trapping set is a collection of an even number of qubits and symmetric stabilizers, such that the induced sub-graph contains no odd-degree stabilizer check nodes. This type of trapping set can always be partitioned into isomorphic disjoint subsets with a set of common odd-degree stabilizer (check) neighborhoods.*

The two disjoint symmetric subsets of the $(6, 0)$ TS, can be identified as $V_a = \{v_0, v_{351}, v_{405}\}$ and $V_b = \{v_{477}, v_{478}, v_{483}\}$. Further, as per the definition III.2. V_a and V_b have the same set of odd-degree stabilizer check neighborhood. That is, $N(V_a) = N(V_b) = \{c_0, c_1, c_6, c_{405}, c_{406}, c_{411}, c_{351}, c_{352}, c_{367}\}$. Following the Lemma 1 from [11], error patterns of cardinality less or equals 3 on any of the subset is a harmful configuration for the $(6, 0)$ TS. For instance any $e_a \subseteq V_a : |e_a| \leq |V_a|$ has an exact twin $e_b \subseteq V_b$. This results into an oscillation between $e_a \oplus e_b$ and an all zero error at each iterations of the *min-sum* decoder discussed in II-D.

Lemma 1. *Iterative decoders with critical number $\frac{n}{2}$ possess no TS characteristics for the $(a, 0)$ QTS, if the cardinality of the error subsets $e_a \subseteq V_a$ or $e_b \subseteq V_b$ exceeds $\frac{n}{2}$.*

Note that, unlike CTS, the common stabilizer neighborhood of the $(6, 0)$ QTS is itself the set of odd degree check nodes for each of the disjoint subsets and therefore emerges as the unsatisfied check nodes satisfying $\text{UNSAT} \subseteq N(V_a) = N(V_b)$. This requires different measures to approach how the iterative message passing can be improved.

B. Use of qubit “separation” to improve iterative decoders

We now show that the iterative decoder can leverage the increased “separation” of the trapped data qubits. We observe that increasing the separation of data qubits has a direct implication towards the decoder’s performance. The oscillatory behavior of the TS discussed in the previous section is majorly contributed by the mis-satisfied check nodes of the TS. For example the $(3, 3)$ TS in Fig 1(a)- c_1, c_6 are the mis-satisfied check nodes for trapped v_0 . The term mis-satisfied justifies the dilemma they produce as they although are satisfied, passes mis-information, resulting in a non-convergence scenario for v_0 . This phenomenon is also reflected in Fig 2. This leads to the intuition behind the separation of a qubit. It is essentially a measure of how far an incorrect trapped qubit is from another trapped qubit in the computation tree [19]. The core notion behind this measure is to identify the mis-satisfied check nodes vulnerable to decoding.

The computation tree (CT) is often used to analyze the performance of iterative decoders in classical settings [19], [20]. Consider a trapping set \mathcal{T}_s , with a set of odd degree data qubits V_1 . It is built either from a trapped qubit $v \in V_1$ or from an unsatisfied check node $c \in C_1$ as a root. From the root, we add descendant check and data qubits according to the iterative message passing (or, the Tanner graph of the

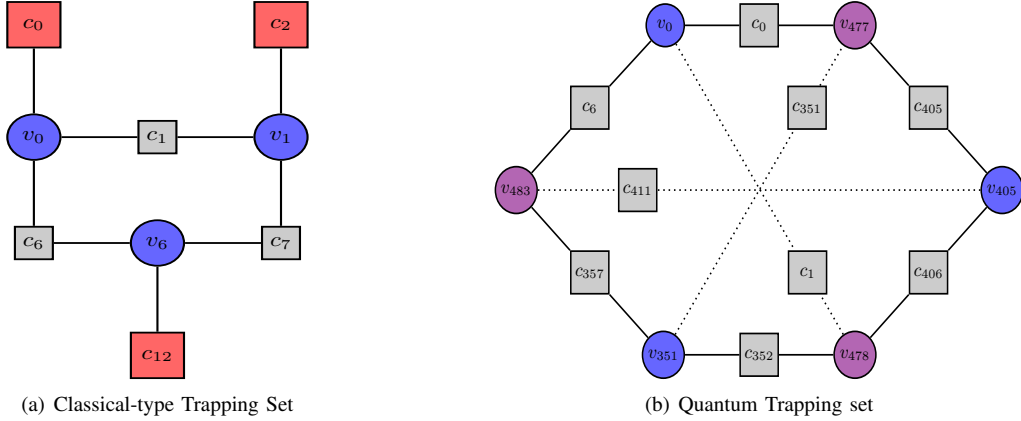


Fig. 1. In (a) we show a typical (3, 3) 6-cycle classical type trapping set and in (b) is a (6, 0) Quantum Trapping set of the $[[882, 24]]$ GHP code.

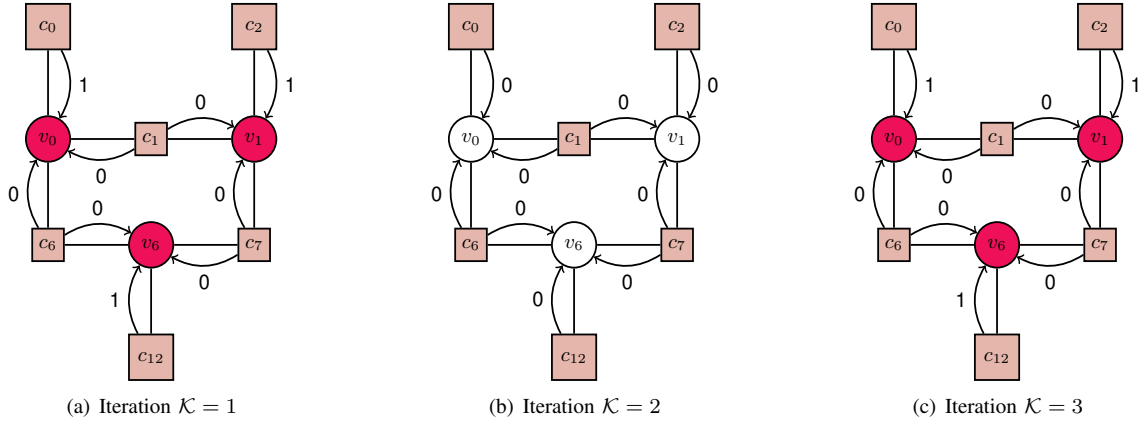


Fig. 2. We show a typical oscillatory behaviour of the *min-sum* BP algorithm (II-D) for the (3, 3) CTS of the $[[882, 24]]$ GHP code. The square colour nodes represent the input unsatisfied check nodes. The final hard information passed to each of the data qubits $v_j \in V_1$ is shown for each complete iteration of the algorithm. Qubits $v_j \notin V_1$ are not affected by the message passing and thus not highlighted. The algorithm is initialized with errors indicated at v_0, v_1 and v_6 . Thereafter, a non-convergent oscillatory behaviour between all zero and $\{v_0, v_1, v_6\}$ is observed.

code). We denote a CT for \mathcal{K} iterations of complete message passing cycles (i.e., qubit \rightarrow check \rightarrow qubit), with a qubit v as root by $T_{\mathcal{K}}(v)$, and if the root is an unsatisfied check node c , then it is denoted by $T_{\mathcal{K}}(c)$. Therefore, \mathcal{K} also indicates the level of the computation tree and from here onward we will alternately use it to denote iteration of the *min-sum* decoder as well as the level of a computation tree. Based on the computation tree of the trapped qubits for both CTS and QTS, the separation of the same is calculated, described in definition III.3 and III.4.

Definition III.3 (Qubit separation for CTS). *If an erroneous data qubit node $v \in V_1$ for any $V_1 \subset \mathcal{T}_s$; has atleast one degree-one check node c , such that, within \mathcal{K} number of message passing iterations of the decoder, there exists no more data qubit $u \in V_1$ as a descendant of c in $T_{\mathcal{K}}(c)$, then the root qubit v is said to be \mathcal{K} separated.*

In Fig. 5 of the appendix, we show the computation tree $T_4(v_0)$ for the (3, 3) CTS. We can see that the qubit v_0 has a separation of $\mathcal{K} = 2$, as at $\mathcal{K} = 3$ there exists $v_6 \in V_1$. Also,

if there are a qubits in \mathcal{T}_s , then separation of each of those qubits represented in an one dimensional vector of length a is called the separation vector of that \mathcal{T}_s . Note at level $\mathcal{K} = 3$ of $T_4(v_0)$, if we remove c_6 , the separation of v_0 is increased to 3, i.e. $\mathcal{K} = 3$ for v_0 . Thus, an increase in separation is intrinsic to the removal of mis-satisfied check nodes. This inturn helps provide good information to the iterative decoders, see appendix VI-A for details. For QTS, we propose a slightly different definition for the *qubit separation*.

Definition III.4 (Qubit separation for QTS). *If a QTS \mathcal{T}_s has degenerate subsets V_a and V_b , then for an erroneous data qubit node $v \in V_a$ with atleast one degree-one check node c , is said to be \mathcal{K} separated, if within \mathcal{K} number of message passing iterations of the decoder, there exists no more data qubit $u \in V_a$ as a descendant of c in $T_{\mathcal{K}}(c)$.*

Similarly, we define the separation for the qubits in V_b . We note that for QTS, the contributions of the harmful information are channelled through the check nodes connecting the disjoint symmetric subsets. These check nodes play the same role

as the mis-satisfied check nodes of the CTS. Although they themselves can be the only unsatisfied check nodes for the harmful error configurations, as we discussed before. In Appendix VI-A, we show for (6,0) QTS, removal of check node pairs from $T_k(v_i)$ (in accordance with definition III.4) has an impact in increasing the separation for v_i , where $v_i, v_j \in \{V_a, V_b\}$. Further, we provide evidences in appendix VI-A, showing that removal of these checks help the iterative decoder predict correct syndromes, which was not possible through the iterative decoder under normal consitions.

In the following section, we first draw an analogy with the classical results from Zhang *et al.* [21] to show that increased separation of a trapped node successfully breaks typical unsuccessful decoding scenarios of the iterative decoder. Further, we perform numerical memory experiments to:

- 1) show the advantage of removing mis-satisfied check nodes through a collaborative decoding approach,
- 2) benchmark the same against *min-sum* BP and state-of-the-art BP+OSD decoder.

IV. DECODING VIA COLLABORATIVE CHECK NODE REMOVAL

As discussed in the previous section, removing the correct check node from the computation tree of a trap node increases its separation and improves the performance of iterative decoders. However, knowing the exact level in the CT from where the check node removal can be done requires the TS information. For example, Fig. 5 in Appendix VI-A shows clearly that the candidate check nodes for removal are in level $\mathcal{K} = 3$ of the CT $T_4(v_0)$. These candidate check nodes are the same mis-satisfied check nodes, information of which can only be known from the TS. Thus, a natural practical way to approach this scenario is through the same probabilistic approach of [13], which increases the separation of the trapped nodes without knowing the particulars of the TS of the quantum code. From here onward, we denote neighbor of a qubit and check as $N(v)$, $N(c)$ respectively and alternately use t and \mathcal{K} for algorithmic syntax purposes.

A. Weak check node removal

From here on we address the decoding algorithm for the CTS. Later, we show generalization to QTS requires modification in the removal rate of check nodes. We saw before that the CTS for the GHP code is rooted in the contribution of a single circulant matrix. For example, the CTS shown in Fig 1(a) is due to the circulant matrix bI_7 . These types of trapping sets have odd-degree check nodes adjacent to them, which we exploit to initialize the decoding. Therefore, we identify the decoding problem as syndrome based and extend the definition of CT construction with unsatisfied check nodes as the roots. Further, we adopt the notion of weak check nodes from [13], which assumes that at any level of $T_{\mathcal{K}}(c)$, $\forall c \in \text{UNSAT}$; there exist at least one weak check node, which is defined in IV.1.

Definition IV.1 (Weak check nodes). *If in level t of the computation tree $T_{\mathcal{K}}(c)$ has a root unsatisfied check node $c \in \text{UNSAT}$, then there exists at-least a check node z , which has the shortest path to any of the nearest qubit $v \in \mathcal{T}_s$, then z is a weak check node at level $\mathcal{K} = t$ of $T_{\mathcal{K}}(c)$.*

Therefore, instead of removing the exact mis-satisfied check nodes from $T_{\mathcal{K}}(v)$, we remove the weak check nodes from level $\mathcal{K} = 1$ of $T_{\mathcal{K}}(c_i)$. It also improves the separation of the adjacent trapped qubit of the unsatisfied check node c_i . For example, Fig 5 in Appendix VI-A shows c_5 as the weak check node at $\mathcal{K} = 1$. Even if the knowledge of (3,3) CTS is unknown, simply removing c_5 from $\mathcal{K} = 1$ of $T_k(c_0)$ can increase the separation of the adjacent qubit v_0 . This helps introduce a lot of freedom and simplicity to the decoding.

Obviously one can remove weak check nodes from any level \mathcal{K} of $T_{\mathcal{K}}(c_i) \forall c_i \in \text{UNSAT}$. Also it is obvious that not all the check nodes at level t are the weak check nodes and removing these will have a negative affect in the further iterative decoding. Therefore, we use the parameter “deselection degree” denoted as *df*, to restrict the number of random check node removal from any level of the CT. Also, note that alternatively one can identify the level $\mathcal{K} = t$ of the computation tree as the level of all leaf check nodes of the computation tree $T_{\mathcal{K}}(c_i)$. This method of removing weak leaf nodes randomly is the key assistive part of the overall decoding architecture. The complete algorithm is known as the *Fixed Node Check Removal* (FNCR) [13], which is described in Algorithm 1.

Algorithm 1: FNCR decoding

```

input :  $\mathbf{H}$ , UNSAT,  $\tau$ , df
output: Modified parity check matrix  $\mathbf{H}_{FN}$ 
1  $\mathbf{H}_{FN} = \mathbf{H}$ ; // Initialization
2  $\text{rem} = []$ ;
3 for check in UNSAT do
4    $\text{leaf} \leftarrow$  All the leaf nodes of  $T_t(\text{check})$ ;
5    $\text{dis} \leftarrow$  random.chose(leaf,df);
6    $\text{rem} \circ \text{dis}$ ;
7 foreach  $\text{uc} \in \text{rem}$  do
8    $\mathbf{H}_{FN} \leftarrow \mathbf{H}_{FN} \setminus \mathbf{H}[\text{uc}]$ ; // Row removal
9 return  $\mathbf{H}_{FN}$ ; // The modified matrix

```

B. Collaborative architecture

For CTS, it is enough to set *df* = 1, as can be seen from Fig. 5 and the numerical results of appendix VI-A. For improving the qubit separation in QTS, ideally, the removal rate should be set to at least *df* = 2, as seen from Fig. 6 in appendix. The modified check matrix output of algorithm 1 has a high probability of having qubits with increased separation and thus offers better convergence with iterative decoders. Therefore, an iterative decoder can be used twice, first with the full parity check matrix and again

on the modified parity check matrix from Algorithm 1. We call this approach a collaborative decoding, details of which are described in Algorithm 2. Collaborative decoding can be considered primarily as using a BP decoder in two modes. During the *main* decoding mode, BP uses the complete parity check matrix of the QLDPC code and the other mode is where it uses the modified parity check matrix output of Algorithm 1, for predicting an error estimate. The later is considered as the *sub*-decoding mode. In Fig 3, we show

Algorithm 2: Collaborative BP decoding with FNCR

input :

- Syndrome:= s and corresponding \mathbf{H} ,
- Channel llr values:= llr ,
- Maximum iterations of primary BP:= \max_{iter} ,
- Maximum iterations of sub BP:= \max_{sub} ,
- Deselection degree: df ,
- Sampling degree: sf ,
- Maximum FNCR rounds: fr ,
- Tolerance of Main BP iterations: tol .

output: Total predicted error pattern \hat{e} .

```

1 unchanged = itn = 0; // Main decoder init
2  $s_{prev} := s$ ;
3 while (unchanged  $\neq$  tol) or (itn <  $\max_{iter}$ ) do
4    $\hat{e}_{bp} = BP(\mathbf{H}, llr, \max_{iter}).decode(s)$ ;
5    $\hat{s}_{bp} = \hat{e}_{bp} \mathbf{H}^T$ ;
6   itn  $\leftarrow$  itn +  $\max_{iter}$ ;
7   if  $\hat{s}_{bp} = s_{prev}$  then
8     unchanged  $\leftarrow$  unchanged + 1
9   else
10    unchanged = 0
11    $s_{prev} \leftarrow \hat{s}_{bp}$ ;
12  $s_{sub} := zeros((fr, \mathbf{H}.shape[0]))$ ;
13  $\hat{e}_{sub} := zeros((fr, \mathbf{H}.shape[1]))$ ;
14 while i < fr do
15   UNSAT = [];
16    $s_{fn} \leftarrow s + \hat{s}_{bp} + (\sum_j s_{sub}[j]), \forall j < i$ ;
17   if check = 0,  $\forall check \in s_{fn}$  then
18     return  $\hat{e} \leftarrow \hat{e}_{bp} + \sum_i \hat{e}_{sub}[i]$ ;
19   End;
20   for check in  $s_{fn}$  do
21     if check  $\neq$  0 then
22       UNSAT.extend(check);
23    $u_s = random.sample(UNSAT, sf)$ ;
24    $\mathbf{H}_{FN} = FNCR(\mathbf{H}, u_s, t, df)$ ;
25    $BP_{sub} = BP(\mathbf{H}_{FN}, llr, \max_{sub})$ ;
26    $\hat{e}_{sub}[i] = BP_{sub}.decode(s_{fn})$ ;
27    $s_{sub}[i] \leftarrow \hat{e}_{sub}[i] \mathbf{H}^T$ ;
28   i  $\leftarrow$  i + 1
29 return  $\hat{e} \leftarrow \hat{e}_{bp} + \sum_i \hat{e}_{sub}[i]$ 

```

the advantage of using BP in the *sub*-decoding mode. We observe, out of numerous sampled instances, a case where the

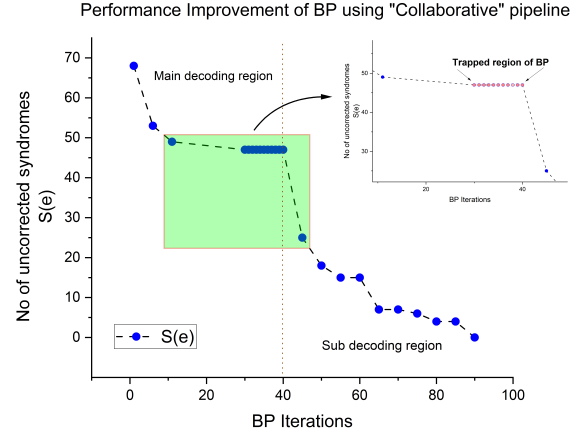


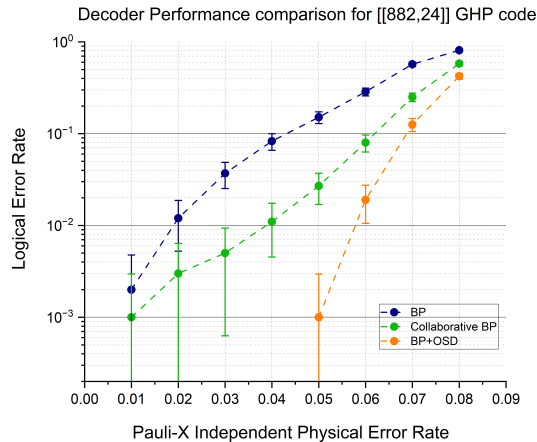
Fig. 3. Numerical experiment showing the *sub*-decoder is able to identify new correct unsatisfied stabilizers, which the main decoder alone can not predict. We observe the decoding performance for the syndrome obtained at independent bit flip physical error rate $p = 0.03$ for $[[882, 24]]$ GHP code. The main BP decoder can not predict any more correct stabilizer violations and gets stuck at 40th iteration. Subsequently, through *sub*-decoding, we call Algorithm 1 repeatedly and BP is applied on the output of the same. We observe repeated calls of Algorithm 1 leads to an improvement to the performance of BP in the *sub*-decoding mode. We also observe a tail in the plot signifying newly accurate predictions of the unsatisfied stabilizer checks.

main BP decoder gets stuck while decoding the syndrome of an error pattern generated at an independent bit flip physical error rate of $p = 0.03$ for the $[[882, 24]]$ GHP code after a few iterations. The stuck scenario represents the fact that the main decoder cannot identify anymore correct stabilizer violations. The tail of the plot shows that by activating the *sub*-decoder, we can predict the syndrome correctly and thus, eventually all the errors are correctly predicted. Therefore, we confirm that removing weak check nodes using Algorithm 1 increases the efficacy of the decoding output.

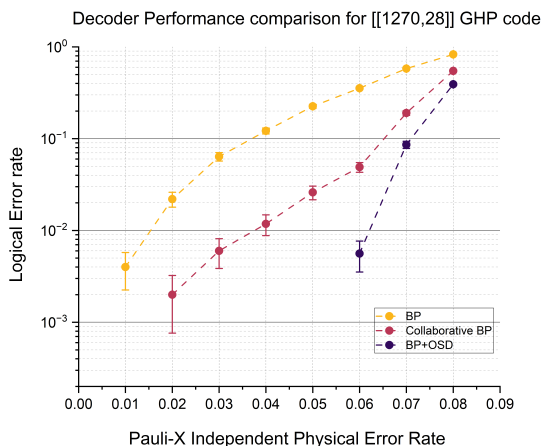
Further, we perform some memory experiments to compare the performance of Algorithm 2 with standard BP *min-sum* decoder and the state-of-the-art BP+OSD decoder. In Fig 4, we show the results, which indicate that the proposed decoding scheme offers significant improvements in the logical error rates over the BP decoder, indicating a potential breakthrough to circumvent the harmful configurations for the iterative BP. Algorithm 2 give logical error rates better than BP but it lags compared to BP+OSD. While BP+OSD uses an exhaustive search strategy to find the most accurate error patterns, Algorithm 2 is devoid of such high-order post-processing steps. There is still a scope to improve accuracy to identify check nodes. For any improvement, we note that the parameter df can help improve the decoding success rates.

C. Time Complexity

The collaborative decoding essentially has two phases, one consisting of the action of BP and the other consisting of the process of modifying the parity check matrix for the sub-



(a)



(b)

Fig. 4. The logical error rates obtained for the GHP codes from [6], under the independent bit flip Pauli channel. We perform the code capacity LER simulations for both cases. In (a) we benchmark with the $[[882, 24]]$ GHP code and in (b) we benchmark the $[[1270, 28]]$ GHP code. The LERs are plotted within a 95% confidence intervals, which are indicated through the error-bars. In both cases, LERs are improved using Algorithm 2 over iterative *min-sum* BP.

decoder. The cost of the latter mainly comes from the process of constructing the computation tree from the unsatisfied check nodes. Now following the concept of weak check nodes, we discussed that a computation tree of level $\mathcal{K} = 1$ is enough to assess the possibility of increasing the separation. For a bi-regular (d_v, d_c) QLDPC code, such a tree construction follows from adding the d_c adjacent data qubits to the root, which is a $\mathcal{O}(n)$ process. Further the leaf check nodes of level $\mathcal{K} = 1$, are added in $\mathcal{O}(m d_c)$ time, where m is the number of stabilizers of the code. As QLDPC codes show extreme sparsity, i.e. $d_c \ll m$, Algorithm 1 or the process of generating the modified check matrix is linear, i.e. $\mathcal{O}(n)$ for a single unsatisfied stabilizer or check node. If the support of the syndrome is $\text{supp}(s) = \|s\|$, then the algorithm has an overall time complexity of approximately $\mathcal{O}(\|s\|n)$. We

also point out that the complexity of Algorithm 1 can even be improved through sampling the unsatisfied check nodes from the syndrome, which essentially reduces the cardinality of the input UNSAT for Algorithm 1. We use the parameter $s\mathcal{F}$, to determine the sampling rate of such unsatisfied check inputs. The collaborative decoder can offer an almost linear computational complexity considering the syndrome weight is low (or, low physical error rate of qubits) or, a heavy sampling of the unsatisfied check nodes. Therefore, the time complexity of the overall collaborative decoding has an implicit dependence on the support of the received syndrome.

V. CONCLUSION AND FUTURE WORK

In this work, we propose a collaborative decoding approach for improving the iterative decoding of QLDPC codes through improving *qubit separation*, with a special focus to GHP codes. We propose a new way to measure the separations of the qubits trapped inside a symmetric stabilizer set. We used this method to go beyond the analysis of qubit separation of the classical trapping sets. Our decoding architecture is free of any post-processing method and can be considered as a two-mode decoder with its main decoder having $\mathcal{O}(n)$ linear complexity. The sub-decoder's complexity depends on support of the syndrome (an implicit dependence on the physical error rates of the qubits). We discussed for practical situations the complexity of the sub-decoder can be improved as much as almost linear. We showed that inspite of being a post-processing-free decoding the success of the algorithm is a significant improvement compared to the standard iterative *min-sum* decoder. In future work, we propose on optimizing the current architecture to restore the lost information due to excessive check node removals thereby approaching better logical failure rates.

DATA AVAILABILITY

The data and scripts used for the numerical experiments are available from the authors on reasonable requests.

ACKNOWLEDGEMENTS

MB acknowledges *ldpc-repository* by Joschka Roffe [22], for sourcing BP and BP-OSD [23] decoders used in the memory experiments. AR and MB thank IISER Bhopal for providing the computational resources to conduct the exhaustive simulations. MB acknowledges the doctoral research fellowship from IISER Bhopal.

REFERENCES

- [1] D. Gottesman, "Fault-tolerant quantum computation with constant overhead," *arXiv preprint arXiv:1310.2984*, 2013.
- [2] P. Panteleev and G. Kalachev, "Quantum ldpc codes with almost linear minimum distance," *IEEE Transactions on Information Theory*, vol. 68, no. 1, pp. 213–229, 2021.
- [3] J.-P. Tillich and G. Zémor, "Quantum ldpc codes with positive rate and minimum distance proportional to the square root of the blocklength," *IEEE Transactions on Information Theory*, vol. 60, no. 2, pp. 1193–1202, 2013.
- [4] P. Panteleev and G. Kalachev, "Asymptotically good quantum and locally testable classical ldpc codes," in *Proceedings of the 54th Annual ACM SIGACT Symposium on Theory of Computing*, 2022, pp. 375–388.

- [5] A. Leverrier and G. Zémor, “Quantum tanner codes,” in *2022 IEEE 63rd Annual Symposium on Foundations of Computer Science (FOCS)*. IEEE, 2022, pp. 872–883.
- [6] P. Panteleev and G. Kalachev, “Degenerate quantum ldpc codes with good finite length performance,” *Quantum*, vol. 5, p. 585, 2021.
- [7] T. Hillmann, L. Berent, A. O. Quintavalle, J. Eisert, R. Wille, and J. Roffe, “Localized statistics decoding: A parallel decoding algorithm for quantum low-density parity-check codes,” *arXiv preprint arXiv:2406.18655*, 2024.
- [8] S. Wolanski and B. Barber, “Ambiguity clustering: an accurate and efficient decoder for qldpc codes,” *arXiv preprint arXiv:2406.14527*, 2024.
- [9] A. GrosPELLIER, L. Grouès, A. Krishna, and A. Leverrier, “Combining hard and soft decoders for hypergraph product codes,” *Quantum*, vol. 5, p. 432, 2021.
- [10] A. K. Pradhan, N. Raveendran, N. Rengaswamy, X. Xiao, and B. Vasić, “Learning to decode trapping sets in qldpc codes,” in *2023 12th International Symposium on Topics in Coding (ISTC)*. IEEE, 2023, pp. 1–5.
- [11] N. Raveendran, “Trapping sets of iterative decoders for quantum and classical low-density parity-check codes,” Ph.D. dissertation, The University of Arizona, 2021.
- [12] Y.-H. Liu and D. Poulin, “Neural belief-propagation decoders for quantum error-correcting codes,” *Physical review letters*, vol. 122, no. 20, p. 200501, 2019.
- [13] S. Kang, J. Moon, J. Ha, and J. Shin, “Breaking the trapping sets in ldpc codes: Check node removal and collaborative decoding,” *IEEE Transactions on Communications*, vol. 64, no. 1, pp. 15–26, 2015.
- [14] N. P. Breuckmann and J. N. Eberhardt, “Quantum low-density parity-check codes,” *PRX Quantum*, vol. 2, no. 4, p. 040101, 2021.
- [15] A. R. Calderbank and P. W. Shor, “Good quantum error-correcting codes exist,” *Physical Review A*, vol. 54, no. 2, p. 1098, 1996.
- [16] A. M. Steane, “Error correcting codes in quantum theory,” *Physical Review Letters*, vol. 77, no. 5, p. 793, 1996.
- [17] A. A. Kovalev and L. P. Pryadko, “Quantum kronecker sum-product low-density parity-check codes with finite rate,” *Physical Review A—Atomic, Molecular, and Optical Physics*, vol. 88, no. 1, p. 012311, 2013.
- [18] D. Chytras, N. Raveendran, and B. Vasić, “Collective bit flipping-based decoding of quantum ldpc codes,” *arXiv preprint arXiv:2406.17070*, 2024.
- [19] B. J. Frey, R. Koetter, and A. Vardy, “Signal-space characterization of iterative decoding,” *IEEE Transactions on Information Theory*, vol. 47, no. 2, pp. 766–781, 2001.
- [20] N. Wiberg, “Codes and decoding on general graphs,” Ph.D. dissertation, Department of electrical engineering, linköping university Sweden, 1996.
- [21] X. Zhang and P. H. Siegel, “Quantized iterative message passing decoders with low error floor for ldpc codes,” *IEEE Transactions on Communications*, vol. 62, no. 1, pp. 1–14, 2013.
- [22] J. Roffe, “LDPC: Python tools for low density parity check codes,” 2022. [Online]. Available: <https://pypi.org/project/ldpc/>
- [23] J. Roffe, D. R. White, S. Burton, and E. Campbell, “Decoding across the quantum low-density parity-check code landscape,” *Physical Review Research*, vol. 2, no. 4, Dec 2020. [Online]. Available: <http://dx.doi.org/10.1103/PhysRevResearch.2.043423>

VI. APPENDIX

A. Computation tree and decoding

Here we explicitly provide the numerical results showing that increasing the separation reflects directly in the improvement of the iterative decoding, which again confirms that removing a mis-satisfied check node has a direct influence on generating “good” information for the iterative decoder.

1) *CTS*: In Fig 5, we show the computation tree for $v_0 \in V_1$ of $(3, 3)$ CTS of $[[882, 24]]$ GHP code. We focus on the descendants of the only odd degree check adjacent to v_0 . The separation of v_0 is 2 as seen from the computation tree. If we follow the red trajectory, removal of c_5 from level 2 or, c_6

from level 3 can increase the separation of v_0 . Following this intuition, all such similar check nodes from level 3, causing a separation of $\mathcal{K} = 2$ are the potential candidate check nodes to be removed. Similarly, if we adopt the notion of weak check nodes, any check node from level 2, having the shortest path to any $v \in V_1$, is also the alternate candidate check node to be removed.

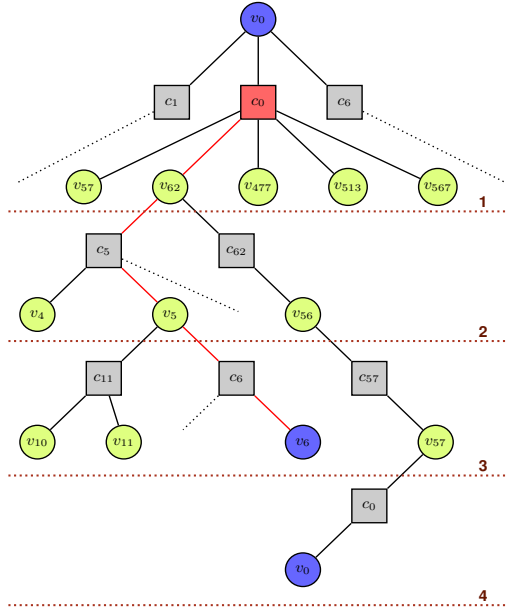
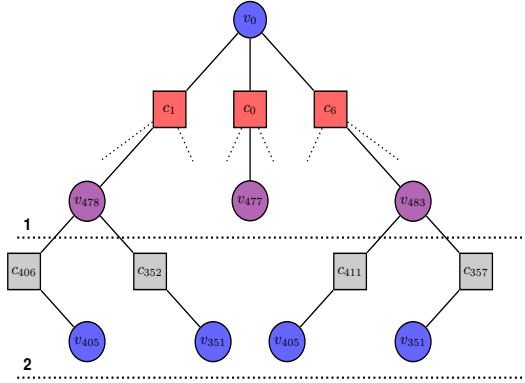


Fig. 5. Computation tree of the trapped qubit v_0 of CTS $(3, 3)$. We show one of the trapped qubits as a descendant of v_0 at layer $\mathcal{K} = 3$ and $\mathcal{K} = 4$.

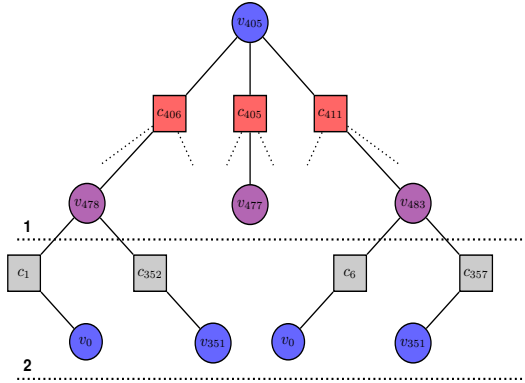
As discussed in Section III and Fig 2, the *min-sum* decoder fails while decoding the syndrome $s = (c_0, c_1, c_2, c_6, c_7, c_{12})$. The oscillatory behavior is unable to predict all the unsatisfied stabilizer checks correctly. In Table I, we show newly corrected unsatisfied check predictions, as we directly remove mis-satisfied check nodes. The checks listed in “Remove check nodes” increase the separation of a trapped qubit. Removal of any of the mentioned check nodes in “Remove check nodes” predicts more correct syndrome bits, which was previously not possible.

2) *QTS*: We also analyze the effect of check node removal on the $(6, 0)$ QTS. From definition III.4, it follows that the separation of a qubit trapped in QTS should be measured based on a particular degenerate set V_a or V_b . For example, in Fig. 6, we show computation trees constructed for $\mathcal{K} = 2$, with v_0, v_{405} and v_{351} as the roots. Firstly, we note that any $v \in V_a$ has only odd degree check nodes, as the full QTS ($V_a \cup V_b$) has no odd degree check nodes. This lays the foundation for not including cross subset nodes in the calculation of the separation. It is due to the fact that removal of the only check nodes connected to the root will leave no scope for the improvement of qubit separation and therefore is not a feasible approach. Thus, our proposed definition III.4 is a rescue for the analysis of the qubits trapped inside any QTS.

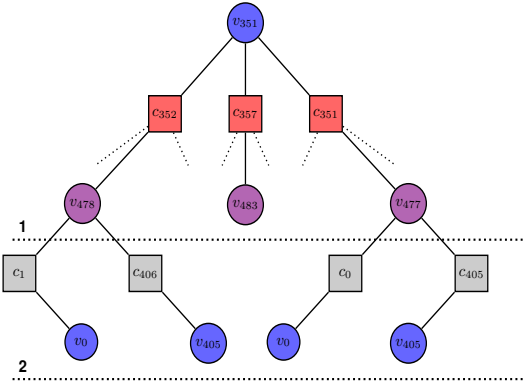
According to definition III.4, we can stretch the computation



(a)



(b)



(c)

Fig. 6. Computation tree and the potential structure indicating the scope of separation improvement for all the trapped qubits of one of the disjoint subset of the $(6, 0)$ QTS of $[[882, 24]]$ GHP code. Note the dotted branches indicated in each of the computation trees. These are the branches bringing flexibility towards separation increments in a QTS enabled by definition III.2. The square check adjacent to leaf blue nodes are the candidate set for removal. The two propositions discussed above can be verified from the diagram.

tree construction for QTS, which is shown in Fig 6. We particularly focus on an error pattern $v \subseteq V_a$, such that the iterative decoder fails to predict the same. For example, an error $e = (v_0, v_{351}, v_{405})$ will result in a decoding failure for the standard *min-sum* iterative BP decoder, showcasing the harmful effect of the QTS. Similar to the CTS, in the present case also all the stabilizers belonging to the QTS,

Code and Trapping set	Separation vector	Remove check nodes	Positively affected trapped qubit	New syndrome bit predictions
$(3, 3)$ CTS of $[[882, 24]]$	$(2, 2, 2)$	c_1 and c_6	v_0	$\{[0, 2, 6, 7], [0, 1, 7, 12]\}$
$(3, 3)$ CTS of $[[882, 24]]$	$(2, 2, 2)$	c_1 and c_7	v_1	$\{[0, 1, 7, 12], [1, 2, 6, 12]\}$
$(3, 3)$ CTS of $[[882, 24]]$	$(2, 2, 2)$	c_6 and c_7	v_6	$\{[0, 1, 7, 12], [1, 2, 6, 12]\}$

TABLE I

DIRECT CHECK NODE REMOVAL SHOWING THE POSITIVE IMPACT ON THE DECODING FOR CTS.

is unsatisfied, the iterative decoder will be unable to predict correct syndrome, due to oscillation between a null and the whole QTS as predictions. In Fig. 6, we observe that removal of check nodes c_{351} and c_{405} will increase the separation of v_0 and similarly the other blue nodes at level 2, offers better separation for each of their corresponding data qubit root node $v \in V_a$. Therefore, any pair of such check nodes are candidates for removal. This analysis directly generalizes for V_b also. In Table II, we show the effect of removing these and certain more check nodes. We report results offering newly corrected stabilizers and therefore confirming the improvement of separation for the qubits trapped in the same QTS. Note that leveraging from the geometry, we further

Code and Trapping set	Remove check nodes	Affected trapped qubits	New syndrome bit predictions by sub-decoder
$(6, 0)$ QTS of $[[882, 24]]$	c_{351} and c_{405}	v_0	$[1, 6, 352, 357, 406, 411]$
$(6, 0)$ QTS of $[[882, 24]]$	c_{352} and c_{406}	v_0	$[0, 6, 351, 357, 405, 411]$
$(6, 0)$ QTS of $[[882, 24]]$	c_{357} and c_{411}	v_0	$[0, 1, 351, 352, 405, 406]$
$(6, 0)$ QTS of $[[882, 24]]$	c_6 and c_{357}	v_{405}	$[0, 1, 351, 352, 405, 406]$
$(6, 0)$ QTS of $[[882, 24]]$	c_1 and c_{352}	v_{405}	$[0, 6, 351, 357, 405, 411]$
$(6, 0)$ QTS of $[[882, 24]]$	c_0 and c_{351}	v_{405}	$[1, 6, 352, 357, 406, 411]$

TABLE II

DIRECT CHECK NODE REMOVAL SHOWING THE POSITIVE IMPACT ON THE DECODING FOR QTS.

draw two direct propositions:

- In QTS, if there exist disjoint symmetric subsets $\{V_i, V_j\}$; then for any $v \in V_i$, the candidate removable check nodes

$\Lambda(c)$, are as follows:

$$\Lambda(c) = \{N(u); \forall u \in V_j, N(u) \cap N(v) = \emptyset, \text{ and } i \neq j\}.$$

- Check node pairs (c_i, c_j) having no common neighbors (i.e. $N(c_i) \cap N(c_j) = \emptyset$) can never be a potential candidate for improving separation of QTS trapped qubits.

B. Numerical Simulation Setup

For benchmarking purpose, we use memory experiments with different GHP codes and decoders. These are monte carlo simulations estimating the logical error rates (LER), for different physical qubit error rates. Also, due to the CSS nature of GHP codes, we perform the experiments for only the *bit flip* errors (i.e. analyzing only the parity check matrix \mathbf{H}_Z). The experiments can similarly be extended for the *phase flip* errors by considering the simulations under the parity check matrix \mathbf{H}_X .

We adopt the code capacity noise model, where each data qubit is expected to suffer bit-flip after a perfect cycle of stabilizer measurements (no gate errors) with probability p . This noise model also assumes that the stabilizer measurements are ideal. Below we briefly elaborate the experimental steps followed:

- 1) Assuming the code has n qubits, we sample a length n vector e , from the binary field for a finite number of shots.
- 2) We Assume the initial state of the code is logical 0: $|0\rangle_L$.
- 3) Estimate the syndrome for each sample, using Eq (2), with \mathbf{H} replaced by \mathbf{H}_z of the QLDPC code and y replaced by e .
- 4) Using a decoder we output a prediction for the error \hat{e} .
- 5) Finally we verify if the residual $e + \hat{e}$ is a stabilizer or a logical operator. In the later we conclude that the decoder failed and produced a net logical error.
- 6) Finally we plot the logical error rates obtained within a certain confidence interval.